Food Packaging and Shelf Life 39 (2023) 101143

Contents lists available at ScienceDirect

Food Packaging and Shelf Life

journal homepage: www.elsevier.com/locate/fpsl

Testing a coated PE-based mono-material for food packaging applications: an in-depth performance comparison with conventional multi-layer configurations

Daniele Carullo [a], Andrea Casson [b], Cesare Rovera [a], Masoud Ghaani [a], Tommaso Bellesia [a], Riccardo Guidetti [b], Stefano Farris [a,*]

[a] DeFENS, Department of Food, Environmental and Nutritional Sciences, Università degli Studi di Milano, via Celoria 2, I-20133 Milan, Italy
[b] DISAA, Department of Agricultural and Environmental Sciences - Production, Landscape, Agroenergy, Università degli Studi di Milano, via Celoria 2, I-20133 Milan, Italy

ARTICLE INFO

Keywords:
Coating
Gas barrier properties
LCA
Transparent plastic materials
UV-Vis spectroscopy
Heat sealing

ABSTRACT

A polyethylene (PE)-based mono-material was considered as an alternative to multi-layer configurations widely used within food packaging sector. An in-depth characterization was performed and several properties (optical, gas/vapor-barrier, and mechanical) tested for the mono-material and selected multi-layer films. The mono-material showed an outstanding performance concerning oxygen ($0.18 \pm 0.01 \bullet 10^{-6}$ mol m^{-2} s^{-1}) and water vapor ($2.84 \pm 0.22 \bullet 10^{-5}$ g m^{-2} s^{-1}) barrier properties, which were ascribed to a thin oxygen barrier coating and the inherent PE hydrophobicity, respectively. The coating also provided excellent UV-C shielding ability, tensile/puncture resistance, and friction properties comparable to those of multi-layer systems. The environmental performance of the materials assessed via LCA showed that the mono-material represented the configuration with the lowest environmental profile. This preliminary work highlighted the potential of PE-based mono-materials functionalized via coating technology as an alternative to multi-layer configurations, thus embracing the increasing demand for more environmentally sustainable solutions (100 % recyclable).

1. Introduction

Over the last few years, the transition toward food packaging solutions fulfilling circularity and sustainability requirements has gained renewed interest, especially due to regulatory pushes (Chang, Trinh, & Mekonnen, 2021; Guerritore et al., 2022; Nuruddin et al., 2021; Santhosh, Nath, & Sarkar, 2021). Within this frame, the academic and industrial sectors have implemented various strategies to ensure high-quality and long-term preservation of food items, with negligible or at least marginal effects on environmental, economic, and social impact possibly arising from packaging materials (Shanmugam et al., 2021; Tyagi, Salem, Hubbe, & Pal, 2021).

Boosted by new legislative initiatives (e.g., directive EU 2019/904 on single-use plastics, now under potential amendment by the Regulation EU 2022/0396/COD) and the growing consumer demand for natural, non-toxic, and possibly biodegradable or compostable solutions, polymeric substrates obtained from renewable resources, namely bioplastics, have recently emerged as an eco-friendly option (Apicella et al., 2019; Farris, Unalan, Introzzi, Fuentes-Alventosa, & Cozzolino, 2014; Gore & Prajapat, 2022; Haghighi, Licciardello, Fava, Siesler, & Pulvirenti, 2020, Kumar, Shukla, Baul, Mitra, & Halder, 2018). Nevertheless, bioplastics still exhibit multiple shortcomings that inevitably slow their spread at the industrial scale, such as poor processability/functionality, as well as scarce economic competitiveness, in comparison with conventional fossil-based materials, together with the lack of sorting options, and weak composting infrastructures (Di Bartolo, Infurna, & Dintcheva, 2021; Kim, Choi, & Jin, 2020; Pinto et al., 2021; Risyon, Othman, Basha, & Talib, 2020; Wu et al., 2019). Accordingly, bioplastics seem a promising option for the next few years as long as the above-mentioned drawbacks are addressed.

Today, in an effort to implement low-environmental-impact packaging configurations, people should consider more efficient and readily available options. From this perspective, improving food packaging materials' recyclability has been included in the key actions for national and regional authorities and industry by the European Commission, which set the goal of ensuring that all plastic packaging is either

* Corresponding author.
E-mail address: stefano.farris@unimi.it (S. Farris).

https://doi.org/10.1016/j.fpsl.2023.101143
Received 18 March 2023; Received in revised form 27 June 2023; Accepted 24 July 2023
Available online 29 July 2023

reusable or can be recycled in a cost-effective manner by 2030 (European Commission, 2018).

Multi-layer configurations represent the most widely adopted solution for many packaged foods because they offer excellent overall performance (e.g., mechanical resistance, thermal properties, and barrier against vapors, gases, and light) by combining several (sometimes up to 11) layers that provide maximum protection. However, as Dilkes-Hoffman et al. (2018) pointed out, multi-layer configurations are very difficult to recycle, especially because of technological hurdles to separate the plastic polymers and the inability to recycle mixed polymers, which often belong to large groups with very different properties (Faraca & Astrup, 2019).

Very recently, mono-materials have been proposed as a potential replacement for multi-layer systems. Several converters (e.g., Amcor plc, 2022; Constantia Flexibles Group GmbH, 2022; ProAmpac, 2022; Schur Flexibles GmbH, 2022; Wipak Group, 2022) have launched new solutions claimed to be valid replacements for multi-layer configurations. Based on the available information, most of these materials consist of a two-layer polyolefin material (polyethylene – PE or polypropylene – PP) whereby a functional coating is sandwiched in between. In the specific case of a PE or PP mono-material, the functional coating first provides the oxygen barrier performance that inherently lacks in polyolefins. To this goal, polymeric water-based coatings are increasingly used. In some configurations, a second coating is used to achieve an extra advantage in terms of water vapor barrier performance beyond that which the polyolefin material is able to provide. In this regard, thin transparent aluminum oxide (Al_2O_3) or silicon oxide (SiO_2) coatings are usually deposited through physically enhanced chemical vapor deposition. In any case, the coating layer is much thinner than the polymer. This thinness explains why these materials formally fall within the heading of "mono-materials", which has to be then confirmed by ad hoc recycling tests that would prove the technical feasibility of the recycling process when using these new mono-materials. Based on the approach the Commission Implementing Decision (EU) 2019/665 adopted, for the purposes of calculating and verifying the attainment of recycling targets, member states are required to report composite packaging and other packaging comprising more than one material but may "derogate from this requirement where a given material constitutes an insignificant part of the packaging unit, and in no case more than 5 % of the total mass of the packaging unit." Many companies and consortia accept this 5 % threshold (such as the Italian Packaging Consortium – CONAI and CEFLEX, a collaborative European initiative representing the entire value chain of flexible packaging).

To the best of our knowledge, no works in the current literature focused on performing a thorough comparison between conventional multi-layer configuration wide-spread in the market and polyolefin-based mono-materials enhanced using an oxygen barrier thin coating. To this end, optical (transparency, UV-Vis transmission, and haze), barrier (carbon dioxide, oxygen, and water vapor), and mechanical (seal strength, tensile/puncture resistance, and static/dynamic coefficients of friction) properties of a coated polyethylene (PE)-based system were investigated and systematically benchmarked with those of pristine PE layers and those of three different multi-layered structures widely used for both fresh and dry products. This choice accounts for an initially broad assessment of the potential of the mono-material for a wide range of applications. Finally, an environmental comparison among tested materials was also performed through life cycle assessment (LCA). The outcome of this study is expected to provide insightful information on the possibility of replacing multi-layer films with high-performance mono-materials for food packaging applications.

2. Materials and methods

2.1. Packaging materials

Four packaging materials were used throughout this study:

1) A mono-material based on polyethylene (PE) provided by O.Kleiner AG (Wohlen, Switzerland) and coded as MM, made of an oriented PE (OPE) layer 25 μm thick coated with a 1.2-μm high-oxygen barrier water-based coating, coupled with an 80-μm LDPE layer by means of a 2-μm adhesive layer (Fig. 1a). Based on the manufacturer's information, the oxygen barrier coating is made of fibres of plant origin.
2) A multi-layer material provided by Cartastampa S.r.l. (Fornaci, Italy) and coded as ML_1, made of four main co-extruded LDPE layers with an ethylene-vinyl-alcohol (EVOH) layer in between, with a 12-μm-thick layer of polyethylene terephthalate (PET) coupled via lamination (Fig. 1b); this type of material can be used for oxygen-sensitive foods, such as cooked ham slices.
3) A multi-layer material provided by Goglio S.p.a. (Daverio, Italy) and coded as ML_2, comprising an 8-μm-thick aluminum sheet sandwiched between an internal sealable LDPE layer (100 μm) and an external printable PET layer (12 μm) by lamination (Fig. 1c); ML_2 is the typical configuration used for ground coffee.
4) A multi-layer configuration provided by Sacchital S.p.a. (Pregnana Milanese, Italy) and coded as ML_3, comprising a 50-μm layer of LDPE coupled with nylon (15 μm) and a 35-μm-thick LDPE/paper printable layer (Fig. 1d). A paper-free area 7 cm in diameter is also present to allow for the clear display of the product inside the package; this kind of configuration is widely used for fresh pasta (e.g., ravioli).

Multi-layer configurations ML_1, ML_2, and ML_3 were used as conventional counterparts of the mono-material MM.

2.2. Characterization techniques

2.2.1. Thickness measurements

The thickness (δ, in μm) of all the investigated plastic materials was first determined using a micrometer (Dialmatic DDI030M, Bowers Metrology, Bradford, UK) with an accuracy of 0.01 μm at 15 random locations. A quantitative description of the films' cross-sectional composition was obtained through optical microscopy (Micro Nikon Eclipse ME600 Laboratory Imaging, Nikon Instruments, Sesto Fiorentino, Italy) at 50 × magnification. Near-rectangular film samples were tightly fixed on a steel sample holder and subsequently cut lengthwise with a sharp razor blade. Image capture/editing and film thickness were measured using the NIS-Element software (Nikon Instruments, Sesto Fiorentino, Italy).

2.2.2. Optical properties

Transparency (T_{550}, in %) and haze (H, in %) were assessed using a high-performance UV-Vis spectrophotometer (Lambda 650, PerkinElmer, Waltham, MA, USA) in accordance with the ASTM D1746 and ASTM D1003. Transparency and haze are important because they describe the packaging material's transparency, that is, the display of the foods inside the package (Unalan, Boyaci, Ghaani, Trabattoni, & Farris, 2016).

To erase any potential influence of the films' thickness, haze values were normalized by the thickness (h, in % μm^{-1}), based on the hypothesis of linearity Fuentes-Alventosa et al. (2013) formulated (Eq. 1):

$$h = \frac{H}{\delta} \tag{1}$$

Last, a quantitative estimation of the UV transmission properties was achieved by collecting transmittance spectra of mono- and multi-layer materials in the wavelength region of 240 – 340 nm (Farris, Introzzi, & Piergiovanni, 2009).

2.2.3. Barrier properties

All polymeric films' carbon dioxide, oxygen, and water vapor barrier properties were investigated on a 50-cm^2 surface sample using a TotalPerm permeability analyzer (ExtraSolution®Srl, Capannori, Italy) based on the isostatic method and equipped with a double sensor

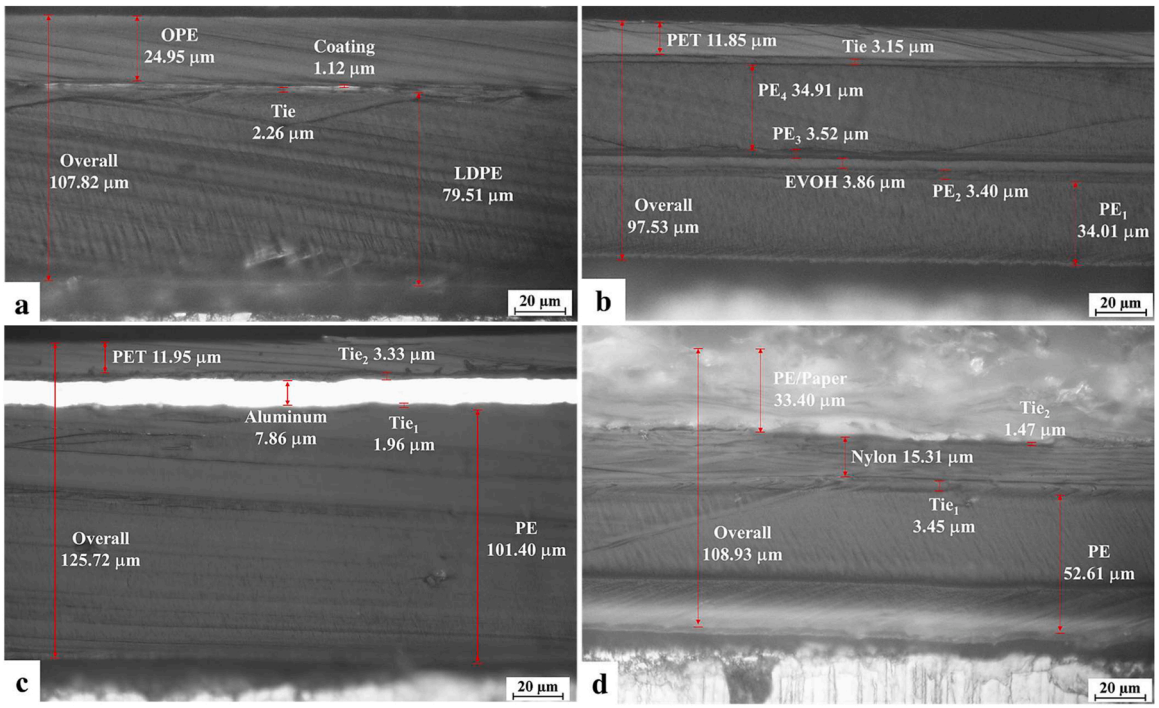

Fig. 1. Cross-sectional optical microscope images (50 × magnification) of MM (a), ML_1 (b), ML_2 (c), and ML_3 (d) materials.

system, that is, an electrochemical sensor for oxygen and an infrared sensor for carbon dioxide and water vapor. The carbon dioxide transmission rate (CO_2TR, in mol m^{-2} s^{-1}) and oxygen transmission rate (O_2TR, in mol m^{-2} s^{-1}) were determined at 23 °C and 50 % relative humidity (RH), according to the standard methods ASTM F2476 and ASTM F2622, respectively, with a carrier flow (N_2) of 10 mL min^{-1} and a one-atmosphere analyte partial pressure difference between the specimen's two sides. For O_2TR, values at a 0.21 partial pressure difference were also calculated with the goal of simulating the oxygen barrier performance under real (atmospheric) conditions. The water vapor transmission rate (WVTR, in g m^{-2} s^{-1}) was measured according to the ASTM F1249 standard method, with a carrier flow (N_2) of 10 mL min^{-1} at 38 °C and 90 % RH (tropical conditions). All the analyses were conducted with each sample's external side (i.e., the side facing the external environment) facing the upper semi-chamber, where the humid test gas (i.e., carbon dioxide, oxygen) was flushed.

Permeability coefficients (Cozzolino, Cerri, Brundu, & Farris, 2014) were obtained from CO_2TR, O_2TR, and WVTR data using the following equation (Eq. 2),

$$P_i^{'} = P_i \bullet \delta = \frac{TR_i}{\Delta p} \bullet \delta \tag{2}$$

where P'_i represents the permeability coefficient (in mol m^{-1} s^{-1} Pa^{-1} or g m^{-1} s^{-1} Pa^{-1}) of the analyte ($i = CO_2$, O_2, and water vapor) and P is the permeance (defined as the ratio of the analyte TR to the difference between the partial pressure of the gas on the film's two sides, Δp). For any considered composite material (MM, ML_1, ML_2, and ML_3), single-layer contributions to the total P'_i values were calculated using the series resistance formula (Eq. 3):

$$\frac{\delta_{tot}}{P_{i,tot}^{'}} = \sum_{j=1}^{n} \frac{\delta_j}{P_{i,j}^{'}} \tag{3}$$

Specifically, δ_{tot} and $P'_{i,\ tot}$ stand for the total material thickness and analyte permeability coefficient, respectively, δ_j and $P'_{i,\ j}$ are the thickness and analyte permeability coefficient of the j-th layer, and n is the total number of layers. For CO_2TR, O_2TR, and WVTR analyses, the final values resulted from five replicates.

2.2.4. Sealing properties

Two 2.54-cm-wide and 15-cm-long strips were generated using a precision sample cutter (mod. MMT, Thwing-Albert, West Berlin/NJ) and heat-sealed on an area of 3.81 cm^2 via a thermal heat sealer (Polikrimper TX/08, Alipack, Pontecurone, Italy) equipped with smooth plates. Pressure and dwell time were fixed according to the typical setup used at industrial scale, as recommended by the films' suppliers, namely, 4.5 bars and 0.5 s, respectively. The sealing temperature was instead investigated between 100 and 170 °C. The maximum temperature corresponded to the point above which all films underwent excessive shrinkage and distortion.

Seal strength (in N) was measured using T-peel tests, following the ASTM F88/F88M-15 standard, which were conducted using a Z005 dynamometer (Zwick Roell, Ulm, Germany) coupled to the software TestXpertV10.11 Master for data elaboration. The system relied on a 100-N load cell and a pair of clamps 20 cm apart (Farris, Cozzolino, Introzzi, & Piergiovanni, 2009). Each run was performed at a crosshead speed of 300 mm/min.

Overall conductive heat transfer coefficients (Green & Perry, 2008) for each analyzed material were calculated according to Eq. (4), which applies only to planar systems:

$$U = \frac{1}{\sum_{j=1}^{n} \frac{\delta_j}{k_j}} \tag{4}$$

where U is the overall heat transfer coefficient (in W m^{-2} K^{-1}) and k_j is the thermal conductivity (in W m^{-1} K^{-1}) of the j-th layer, evaluated at 25 °C (Table S1 of the Supplementary Material).

2.2.5. Mechanical properties

Mechanical properties were assessed using a dynamometer (model Z005, Zwick Roell, Ulm, Germany) and the software TestXpert V10.11 for data analysis. In the case of the tensile properties, the elastic modulus (E_T, in MPa), the elongation at break (ε_B, in %), and the tensile strength (TS, in MPa) were determined on film strips 15 cm in length and 2.54 cm in width, according to ASTM D882. Tests were conducted employing a 5-kN load cell connected with two clamps 10 cm apart.

Puncture tests were conducted according to ASTM F1306, using specimens with a 6-cm diameter punctured by a hemispherical (biaxial stress) probe with a 3.2-mm diameter. Load cell nominal capacity and probe speed during the test were 100 N and 25 mm/min, respectively. The samples' resistance to puncturing was evaluated in terms of elastic modulus (E_C, in MPa), maximum force (F_{MAX}, in N), and work of rupture (W, in mJ).

Static (μ_S) and dynamic (μ_D) coefficients of friction (COF) of films were determined according to ASTM D1894 in typical "plastic vs plastic" and "plastic vs. metal" configurations. In particular, the former allowed for the evaluation of the friction opposing the motion of each type of material against itself whereas the latter was intended to simulate the friction between the plastic web and the metallic parts of the equipment used during the manufacturing process (Farris, 2018). For any investigated parameter, the final mean of the results is calculated from at least five replicates.

2.2.6. Environmental performance

A comparative environmental analysis of the packaging materials was conducted using the life cycle assessment methodology. The declared unit, identified as the reference unit of the system analyzed, was defined as 1 m^2 of packaging material to allow for comparison of the packaging material options. The system boundaries followed a "cradle-to-gate" approach, and the life cycle assessment included all the activities from raw material extraction to packaging film creation. The entire explorative LCA study was based on secondary data, except for those obtained from the characterization of the films. Ecoinvent 3.8 was used as the only database source for the films and layers evaluated. To conduct the environmental impact assessment, SimaPro v 9.4. (PRé Sustainability, Amersfoort, The Netherlands) software was used. In accordance with the literature, the impact assessment methodology used was CML-IA, an LCA methodology the Center of Environmental Science (CML) of Leiden University in The Netherlands developed.

2.3. Statistical analyses

All analyses were conducted at least three times unless otherwise specified. The mean values and standard deviations of the experimental data were calculated. Statistically significant differences among the averages were evaluated using a one-way analysis of variance and Tukey's test ($p \leq 0.01$). Statistical analysis was conducted using IBM SPSS Statistics 20 software (IBM Corp., Armonk, New York, USA).

3. Results and discussion

3.1. Packaging materials' optical properties

The nature of the packaging system and its interaction with light may significantly contribute to the quality preservation and appearance of contained food products (Farris et al., 2009a; Farris et al., 2021). We, therefore, investigated the materials' optical properties with the goal of comparing the coated films' performance with that of the conventional multilayer structures selected as reference materials (Table 1).

As Table 1 shows, the MM sample's transparency did not significantly ($p > 0.01$) differ from the transparency of the commercial solutions, namely ML_1 and paper-free ML_3. If we consider OPE's and LDPE's individual effects (see Table S2 of the Supplementary Material) on the final T_{550} value of MM, it can be inferred that the deposition of the thin coating layer on the 80-μm LDPE sheet (Fig. 1a) did not affect the material's final transparency. Analogous conclusions were drawn by Nuruddin et al. (2021), who evaluated the impact of cellulose nanocrystals (CNCs)/polyvinyl alcohol (PVA) coatings on polypropylene (PP) films. Regardless of the employed CNCs/PVA mass ratio, the authors did not detect any worsening effect on PP transparency after the deposition of the coating, which was explained by the absence of defects, voids, and nonuniformities when the protective layer was spread out onto the original substrate.

Regarding the haze of films, ML_1 and paper-free ML_3 systems exhibited the lowest H values. This finding can be explained in consideration of the greater thickness of the haze-contributing layers (OPE and LDPE) in the MM configuration compared to the ML_1 and ML_3 systems, whereby PET and Nylon do not significantly affect the final haze values (Farris et al., 2009a). In fact, haze has been demonstrated to vary linearly with an increasing number of scattering centers (e.g., crystalline domains), which increase with the material's thickness (Fuentes-Alventosa et al., 2013). Interestingly, the coating's presence in the sample MM did not affect the haze. To demonstrate that, we postulated quantifying a multi-layer material's haze as the sum of the contribution arising from each individual layer interfering with the linear penetration of light (Eq. 5) (Introzzi et al., 2012a):

$$H_{multi-layer} = \sum_{i=1}^{n} h_i \bullet \delta_i \quad (5)$$

Taking this into account, the total haze for a bi-layer material made of an 80-μm LDPE and a 25-μm OPE achieves a theoretical value of 18.7 %, which is slightly higher than that reported with the coated sample (16.7 %). This result confirms the neutrality of the employed coating on the final H value of the MM sample, thus supporting the previously discussed data on transparency (Table 1). Moreover, the slightly lower experimental value of haze compared to the predicted one can be plausibly explained in terms of polysaccharide coatings' antireflective behavior, as previously seen in pullulan coatings (Introzzi et al., 2012b; Cozzolino, Castelli, Trabattoni, & Farris, 2016b). It is also worth noting that none of the tested materials exceeded 30 % in haze; that is, no translucency was detected (Trossaert, De Vel, Cardon, & Edeleva, 2022). Finally, it must be pointed out that the ML_2 packaging was kept out of this discussion because an aluminum sheet does not allow light to pass through the material (Ayieko et al., 2015).

Fig. 2 displays the UV transmission spectra of samples MM and ML_{1-3}. Although a completely flat curve was obtained from the sample ML_2 (i.e., no light was transmitted across the sample), the monomaterial had a pronounced UV-shielding behavior below 280 nm. Considering that the individual films of the sample MM had UV transmittance values above 80 % throughout the scanned wavelength region

Table 1
Optical and permeability properties of the different materials tested in this work.

Material	Optical properties			Permeability properties				
	T_{550} [%]	H [%]	h [% μm^{-1}]	$10^6 \bullet CO_2TR$ [mol m^{-2} s^{-1}]	$10^6 \bullet O_2TR$ [mol m^{-2} s^{-1}]	$10^6 \bullet O_2TR_{AIR}$ [mol m^{-2} s^{-1}]	$10^5 \bullet WVTR$ [g m^{-2} s^{-1}]	CO_2TR/O_2TR
MM	89.1 ± 0.7^{ab}	16.7 ± 1.4^{a}	0.155	4.76 ± 0.20^{a}	0.18 ± 0.01^{a}	0.04 ± 0.01^{a}	2.84 ± 0.22^{a}	26.28
ML_1	87.8 ± 0.1^{a}	7.9 ± 0.2^{b}	0.079	1.75 ± 0.21^{a}	0.25 ± 0.02^{a}	0.05 ± 0.01^{a}	3.09 ± 0.41^{a}	7.08
ML_2	N.A.	N.A.	N.A.	< LDL	< LDL	< LDL	< LDL	N.A.
ML_3	89.4 ± 0.1^{b}	9.2 ± 0.3^{b}	0.081	84.95 ± 8.19^{b}	14.05 ± 1.54^{b}	2.95 ± 0.32^{b}	6.92 ± 0.63^{b}	6.05

The results are expressed as mean ± SD. For each investigated parameter, different lowercase letters within the same column express significant differences ($p < 0.01$) among mean values. Legend: N.A. = not applicable, LDL = lower detection limit ($1.29 \bullet 10^{-7}$ mol m^{-2} s^{-1} for CO_2TR, $5.2 \bullet 10^{-9}$ mol m^{-2} s^{-1} for O_2TR, $1.1 \bullet 10^{-9}$ mol m^{-2} s^{-1} for O_2TR_{AIR}, and $2.5 \bullet 10^{-8}$ g m^{-2} s^{-1} for WVTR).

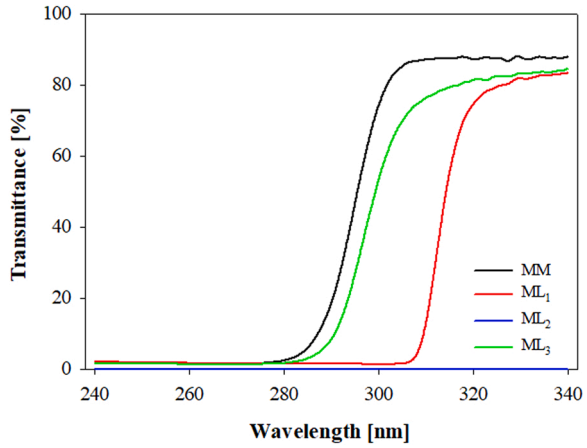

Fig. 2. UV-Vis transmission spectra of the materials tested in this work.

(see Fig. S2 of the Supplementary Material), it can be concluded that the UV-blocking effect of the material MM for wavelengths < 280 nm was due to the coating's presence. A slightly better performance was observed for the sample ML_3 (Fig. 2) due to the UV absorption capability of chromophore carbonyl groups distributed along the nylon chains (Berova, Di Bari, & Pescitelli, 2007). This performance further increased for the same material when the multilayer included paper (Fig. S3 of the Supplementary Material). Among the tested materials, sample ML_1 guaranteed the best UV protection, where the cut-off at approximately 310 nm was attributed to the aromatic ring of PET (Rizzo, Torri, Licciardello, Piergiovanni, & Muratore, 2015). From these results, it can be envisaged a boosting in the coating's UV-blocking effect to improve the protection, for example, against the artificial lights employed in retail stores (Farris et al., 2009a).

3.2. Barrier properties of packaging materials

Packaging materials' permeation of gases and vapors plays a key role in determining a food product's perishability (thus the shelf life). For this reason, gas and vapors transfer phenomena occurring across the packaging material must be considered with attention when designing packaging configurations with tailored performance according to the specific application (Farris, 2018).

Table 1 shows the carbon dioxide, oxygen, and water vapor transmission rates from all the investigated samples, together with the CO_2TR/O_2TR permselectivity coefficients. The mono-material MM showed an excellent oxygen barrier performance owing to the thin coating between the two polyolefins, which conversely showed permeability values of approximately 4 orders of magnitude higher than the laminate thereof (Table S3 of the Supplementary Material). Polyolefins' poor barrier performance against oxygen has been explained in terms of intrinsic hydrophobicity, which hinders both polar-to-polar interactions and hydrogen bonding (Wang et al., 2018). These results are consistent with previous reports on the physicochemical evaluation of neat and functionalized polyolefins for food packaging applications (Farris et al., 2009a; Farris, 2018; Huang, Guo, Zhang, Zhang, & Guo, 2013; Pinto et al., 2021). Polyolefins' inherent hydrophobicity ensured the MM sample with very good moisture barrier properties, which are crucial to keep the coating's oxygen barrier performance at good levels even at high (e.g., 80 %) RH values.

The performance of the mono-material seemed to equalize that of sample ML_1 including an EVOH layer, which is thus far the most preferred commercial solution when a high oxygen barrier performance is sought. However, a deeper analysis of the permeability coefficients of the individual layers forming both MM and ML_1 (Table S4 of the Supplementary Material) revealed that LDPE, OPE, and PET have very high P'_{CO2} and P'_{O2} values ($\approx 10^{-15}$–10^{-12} mol m^{-1} s^{-1} Pa^{-1}), suggesting that both the coating and the EVOH layer were responsible for the limited transfer of carbon dioxide and oxygen across the films (Table 1). However, it is interesting to note that the coating of the sample MM possessed a superior CO_2- and especially O_2-barrier performance than EVOH did, as easily gained from the results of Table S4 of the Supplementary Material (91 % and 76 % reduction in P'_{CO2} and P'_{O2} values, respectively, below that of the ML_1 multi-layer). Finally, a comparison between samples MM and ML_1 concerning the WVTR parameter revealed that both materials performed well with very similar values. For both materials, the limiting polyolefin layers governed this performance (that is, OPE and LDPE for the sample MM and LDPE for the sample ML_1, see Table S4 of the Supplementary Material).

Sample ML_3 showed an inferior oxygen barrier performance compared to both MM and ML_1 (Table 1). This performance can be explained by the presence of a 15-μm thick nylon sheet, which is well known to have good (but not excellent) oxygen barrier properties (Finnigan, 2009), whereas the highly porous structure of the cellulosic layer did not offer any appreciable resistance against the diffusion of gases (Rovera, Türe, Hedenqvist, & Farris, 2020). In a similar way, the WVTR of the sample ML_3 was higher than that detected in MM and ML_1 samples. In this case, the main reason lies in the lower thickness of the moisture-limiting layers (polyolefins) of sample ML_3 (60 μm) as compared to the mono-material MM (105 μm) and the sample ML_1 (87 μm). As previously seen for the optical properties, the sample ML_2 was the best-performing solution among those considered in this work also as far as the permeability performance was concerned. This is because any mass transfer phenomenon across the aluminum foil of the laminate is totally blocked or, at least, below the lower detection limits of the utilized instrument (Table 1).

3.3. Mechanical properties of packaging materials

Fig. 3 depicts the seal strength versus temperature curves originating from T-peel tests of multi-layer packaging materials. As a general trend, sealing temperatures lower than 130 °C did not guarantee adequate strength, probably due to incomplete melting of the PE sheets for all the multi-layer materials, as previous literature evidence supports (Zia, Paul, Heredia-Guerrero, Athanassiou, & Fragouli, 2019). In contrast, more severe thermal conditions triggered a progressive ($p < 0.01$) increase in the seal strength up to 150 °C. Further rises in temperature above this point scarcely affected the seal strength, which then tended to level off to a constant value. Interestingly, the ML_2 sample deviated from the above observations because the first, significant seal strength was

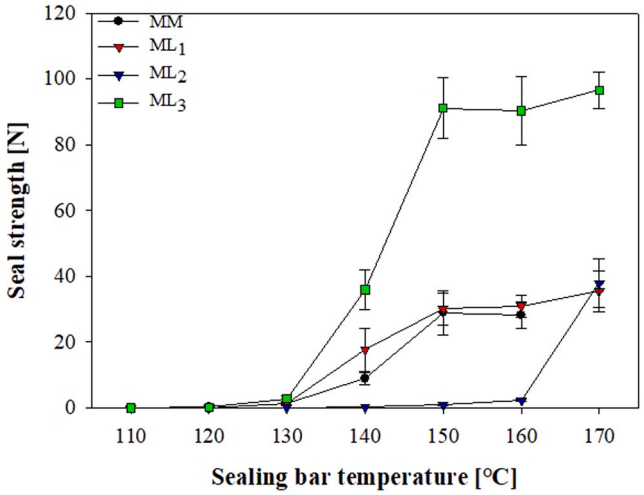

Fig. 3. Seal strength as a function of temperature for the materials tested in this work. Error bars indicate standard deviations around the mean values ($p < 0.01$).

measured at the highest temperature (170 °C). It must be also inferred that, regardless of the considered material, a typical "tearing" failure mode was found (data not shown).

A comparative analysis of the overall heat transfer coefficients (Eq. 4) enabled gaining additional insights into the behavior of tested materials after sealing. As reported in Table S6 of the Supplementary Material, the highest *U* values for MM and ML_1 are reflected in seal strength values significantly higher ($p < 0.01$) than those shown by the Al-based material (ML_2) up to 160 °C. Accordingly, the lowest *U* value for the ML_2 system would explain the less efficient heating of ML_2 upon sealing, at least for the process duration applied in this work (0.5 s). This led to an incomplete melting of PE, thus to low seal strength values, at least up to 160 °C. However, a deviation from the relationship between *U* values and seal strength values has been observed for the paper-covered ML_3 material, which has shown the best sealing strength performance throughout the thermal range considered (Fig. 3), despite its low *U* value (Table S6 of the Supplementary Material). As already discussed, this apparently anomalous behavior can be explained by considering the different specific heat capacity of cellulose and plastic layers (Lavrykov, & Ramarao, 2012; Zarandi, Bioki, Mirbagheri, Tabbakh, & Mirjalili, 2012) forming the ML_3 material. An extensive investigation on the effect of packaging materials' heterogeneity on heat transfer efficiency is thus necessary to clarify the different performances of multi-layer materials during sealing operations.

Tensile properties of multi-layer materials (Table 2) have been evaluated in both machine and transverse directions (MD and TD, respectively), which have been found to affect the multi-layer materials' final tensile performance (Song et al., 2022). For all materials, the MD-tested samples showed significantly ($p < 0.01$) higher values in E_T and TS than those extracted along the transverse direction. Regarding the MM mono-material, its tensile properties arise from the combination of LDPE and OPE. Notably, the OPE sample exhibited a much higher stiffness regarding the unoriented LDPE (Table S7 of the Supplementary Material) as a result of the stretching and alignment of polymeric chains upon orientation, which eventually resulted in intensifying the crystalline features over the amorphous ones (Tyun'kin, Bazhenov, Efimov, Kechek'yan, & Timan, 2011). The elastic modulus of the MM mono-material was the lowest recorded among all the multi-layer films tested in this work, which reflects the polyolefins' less stiff behavior compared to Al/PET (ML_2) and nylon/cellulose (ML_3) combinations, well known for their superior rigidity (Cozzolino, Campanella, Ture, Olsson, & Farris, 2016a; Luzi, Torre, Kenny, & Puglia, 2019; Sharif et al., 2021).

Regarding the resistance of the material to puncture stresses, it has been observed a trend very similar to that of the tensile test, with a higher resistance to penetration shown by ML materials rather than the MM configuration, as demonstrated by the significantly ($p < 0.01$) higher values in the investigated puncture parameters (Table 2). In particular, the PE/nylon/PE-paper material (ML_3) showed the best performance in energy absorption upon punctural compression, confirming the best performance of polyamides (e.g., nylon 6,6 or nylon 6,12) over polyolefins to withstand punctural stresses that may occur during logistic operations or at retailers' level (Firouzi, Foucher, & Bougherara, 2014). Concerning the MM sample, it benefited from an almost additive effect in terms of E_C and F_{MAX} from the two layers of which it is made (i.e., OPE and LDPE). Conversely, the W parameter was closer to that of the LDPE rather than OPE (Table S8 of the Supplementary Material). This can be explained considering that the stiffer behavior of oriented polyethylene dramatically curbed the major extensibility of LDPE, leading to a consistent reduction in the deformation at rupture; hence, in the area below the curve of the MM sample (Fig. S4 of the Supplementary Material).

Finally, regarding the friction properties, all the materials tested in this study displayed COF values falling within the 0.2–0.4 range deemed acceptable at the industrial level for proper in-line operations (e.g., winding/unwinding) (Table 2). The only exception concerned the multi-layer ML_1 for the "int. to int." test, which had a static coefficient of friction of 0.55, very high considering the two facing layers are LDPE. Similarly, the same coefficient was found higher than expected for the mono-material MM under the same test ($\mu_S = 0.35$). This value is somehow unexpected considering that μ_S of the LDPE used for the MM manufacturing was approximately 0.2 (Table S9 of the Supplementary Material). A plausible explanation for this behavior can be the excessive treatment for the surface activation of LDPE before the deposition of a layer such as adhesives, coatings, inks, and others. When the treatment (i.e., corona treatment, flame treatment, or plasma) is run beyond a certain limit, it can extend over the first micron of the web's surface, thus almost reaching the opposite side of the same web. This phenomenon is known as the "back side effect" and it is particularly known for corona-treated plastic substrates.

3.4. Environmental performance properties

Fig. 4 proposes a comparison of the results that come from the

Table 2
Values of the main parameters obtained from the tensile, puncture, and friction tests on the materials tested in this work.

Material	Tensile parameters				Puncture parameters		
	Direction	E_T [MPa]	ε_B [%]	TS [MPa]	E_C [MPa]	F_{MAX} [N]	W [mJ]
MM	MD	600 ± 20^{a}	$*102.0 \pm 4.4^{b}$	$*38.2 \pm 2.8^{c}$	6.0 ± 0.2^{a}	16.3 ± 0.4^{a}	44.0 ± 4.6^{a}
	TD	561 ± 40^{A}	$*247.5 \pm 30.5^{D}$	$*12.8 \pm 0.8^{A}$			
ML1	MD	1005 ± 62^{b}	65.5 ± 2.5^{a}	$*34.8 \pm 0.9^{b}$	9.5 ± 0.4^{b}	25.8 ± 1.2^{b}	62.7 ± 6.0^{b}
	TD	907 ± 41^{B}	67.0 ± 4.3^{C}	$*29.6 \pm 0.9^{B}$			
ML2	MD	$*1539 \pm 96^{c}$	$*65.1 \pm 7.4^{a}$	32.3 ± 2.1^{ab}	10.6 ± 0.8^{c}	30.5 ± 1.6^{c}	77.6 ± 8.2^{c}
	TD	$*1165 \pm 95^{C}$	$*28.9 \pm 6.6^{A}$	29.8 ± 1.3^{B}			
ML3	MD	$*1663 \pm 180^{c}$	$*101.8 \pm 17.1^{b}$	28.4 ± 2.2^{a}	9.1 ± 0.2^{b}	36.6 ± 1.8^{d}	127.6 ± 10.8^{d}
	TD	$*872 \pm 70^{B}$	$*37.8 \pm 5.7^{B}$	30.4 ± 2.9^{B}			

Material	Static and dynamic coefficients of friction									
	$Film_{int\text{-}to\text{-}filmint}$		$Film_{ext\text{-}to\text{-}filmext}$		$Film_{int\text{-}to\text{-}filmext}$		$Film_{int\text{-}to\text{-}metal}$		$Film_{ext\text{-}to\text{-}metal}$	
	μ_S	μ_D	μ_S	μ_D	μ_S	μ_D	μ_S	μ_D	μ_S	μ_D
MM	0.35 ± 0.06^{b}	0.32 ± 0.01^{b}	0.31 ± 0.01^{ab}	0.21 ± 0.01^{b}	0.28 ± 0.01^{b}	0.20 ± 0.01^{a}	0.28 ± 0.01^{a}	0.22 ± 0.01^{a}	0.25 ± 0.01^{a}	0.14 ± 0.01^{a}
ML1	0.55 ± 0.05^{c}	0.35 ± 0.01^{b}	0.30 ± 0.02^{ab}	0.21 ± 0.01^{b}	0.36 ± 0.01^{c}	0.27 ± 0.01^{c}	0.34 ± 0.01^{b}	0.27 ± 0.01^{b}	0.32 ± 0.02^{b}	0.20 ± 0.01^{b}
ML2	0.20 ± 0.02^{a}	0.18 ± 0.02^{a}	0.27 ± 0.02^{a}	0.20 ± 0.01^{b}	0.23 ± 0.01^{a}	0.19 ± 0.01^{a}	0.30 ± 0.03^{ab}	0.23 ± 0.01^{a}	0.31 ± 0.03^{b}	0.19 ± 0.01^{b}
ML3	0.21 ± 0.02^{a}	0.16 ± 0.02^{a}	0.33 ± 0.02^{b}	0.17 ± 0.01^{a}	0.29 ± 0.01^{b}	0.23 ± 0.01^{b}	0.29 ± 0.02^{a}	0.23 ± 0.01^{a}	0.42 ± 0.03^{c}	0.23 ± 0.01^{c}

The results are expressed as mean ± SD. For each investigated parameter, different lowercase letters within the same column express significant differences ($p < 0.01$) among mean values. For the tensile parameters, different letters within the same column and for each specific parameter express significant differences ($p < 0.01$) between materials when evaluated in MD (lowercase letters) or TD (uppercase letters), respectively. The symbol * indicates a significant difference ($p < 0.01$) between MD and TD within a same material. For the friction properties, the subscripts "int" and "ext" refer to the internal side (i.e., the side facing the food inside a package) and external side (i.e., the side in contact with the environment) of the materials, respectively.

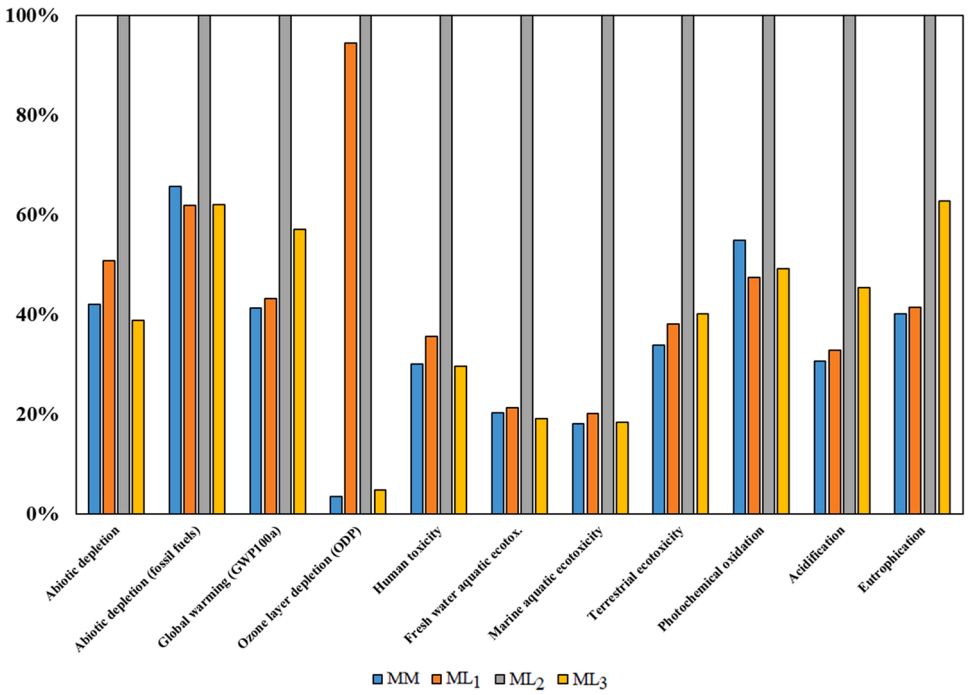

Fig. 4. Environmental performance of the four packaging solutions investigated in this study (quantitative evaluation available in Table S9 of Supplementary Material).

explorative LCA study of the four packaging solutions. The 11 environmental impact categories are reported on the x-axis, while a percentage value is presented on the y-axis. The worst-case scenario for each impact category reaches 100 %, while the others are scaled relative to it. The results reveal that the ML_2 solution reflects the worst scenario in all the impact categories, reaching 100 % in all of them. ML_1 represents a better solution compared to ML_2 (−56 % impact on average among impact categories) but not the best solution. ML_3 and MM are the packaging solutions with the lower environmental profile, respectively −61 % and −65 % (on average among impact categories) of impact compared to the ML_2 solution. The environmental impact of the four packaging solutions is heavily influenced by their composition, both in terms of the type of materials used and grammage (mass per unit area, g/m^2), which can be identified as hotspots.

A detailed description coming from the factors that can affect the environmental impact of the four different packaging solutions (i.e., raw materials – upstream operations – and energy consumption for lamination/drying steps, expressed as electrical energy) is proposed in Figs. S5-S8 of the Supplementary Material. In particular, considering the ML_2 option and its environmental footprint (Fig. S5 of the Supplementary Material), the presence of the aluminum layer highly influences the environmental impact of this solution. In fact, this layer accounts for an average of 49 % of the impacts. Considering the other options, they are characterized by a more even distribution of the environmental load among the individual polymeric layers. In particular, for the configuration ML_1 (Fig. S6 of the Supplementary Material), the highest contribution among impact categories comes from the PET layer (29 % among impact categories), the PE layers (20 % among impact categories), and the energy consumption for the film manufacturing (16 % among impact categories). For the ML_3 solution (Fig. S7 of Supplementary Material), the hotspots are the PE layers (38 % among impact categories), the PE/paper layer (21 % among impact categories), and the Nylon layer (20 % among impact categories). Finally, regarding the mono-material MM (Fig. S8 of Supplementary Material), note that the LDPE and OPE layers together accounted for 89 % (67 % and 21 %, respectively) of the contribution of the whole packaging solution environmental impact.

Besides any analytical evaluation, it must also be considered that complex systems such as ML_2, ML_3, and ML_1 (which involve materials of different nature and different manufacturing processes) cannot undergo efficient recycling and virtuous end-of-life management options, being in most cases disposed of in the unsorted waste. Conversely, the MM solution offers new opportunities in terms of environmental performance, provided that specific recycling test will be carried out to assess the technical feasibility of the extrusion of the PE-coated material. For example, as a mono-material, it can be considered as fully fitting with the eco-design approach, representing a solution with high recyclability performance.

4. Conclusions

This explorative study highlighted the potential of mono-materials based on polyolefins to replace conventional multi-layer configurations for the packaging of both fresh (e.g., cooked ham, and fresh pasta), or dry (e.g., roasted coffee) food products. In particular, we have shown that sandwiching a thin coating layer between LDPE and OPE sheets enables generating a new mono-material with similar or even better functional properties of common multi-layer solutions regarding barrier properties, heat sealability, and overall mechanical performance. Not less important, the mono-material option offers better performance regarding environmental impact, which is increasingly recognized as a requisite for new packaging solutions. To validate the outcome of the present research, additional shelf-life studies on different food product categories will be carried out so that the environmental performance of the PE-based mono-material presented in this work will be verified also in terms of food losses.

CRediT authorship contribution statement

D. Carullo: Conceptualization, Data curation, Formal analysis, Investigation, Methodology, Writing - original draft. **A. Casson:** Formal analysis, Methodology, Writing - original draft. **C. Rovera**: Methodology, Supervision, Writing - review & editing. **M. Ghaani, and T. Bellesia**: Writing - review & editing. **R. Guidetti:** Writing - review & editing. **S. Farris**: Conceptualization, Methodology, Funding

acquisition, Supervision, Project Administration, Writing - review & editing.

Declaration of Competing Interest

The authors declare that they have no known competing financial interests or personal relationships that could have appeared to influence the work reported in this paper.

Data availability

The data will be made available upon request.

Acknowledgments

This research work was carried out via the co-financing of the European Union – FSE, Research & Innovation 2014–2020 National Operative Program (Contract code: 15-G-13883-1).

Appendix A. Supporting information

Supplementary data associated with this article can be found in the online version at doi:10.1016/j.fpsl.2023.101143.

References

Amcor plc, 2022. https://www.amcor.com/sustainability/products. (Accessed October 2022).

Apicella, A., Scarfato, P., Di Maio, L., & Incarnato, L. (2019). Sustainable active PET films by functionalization with antimicrobial bio-coatings. *Frontiers in Materials, 6*, 243. https://doi.org/10.3389/fmats.2019.00243

Ayieko, C. O., Musembi, R. J., Ogacho, A. A., Aduda, B. O., Muthoka, B. M., & Jain, P. K. (2015). Controlled texturing of aluminum sheet for solar energy applications. *Advances in Materials Physics and Chemistry, 5*, 458–466. https://doi.org/10.4236/ampc.2015.511046

Berova, N., Di Bari, L., & Pescitelli, G. (2007). Application of electronic circular dichroism in configurational and conformational analysis of organic compounds. *Chemical Society Reviews, 36*, 914–931. https://doi.org/10.1039/b515476f

Chang, C. C., Trinh, B. M., & Mekonnen, T. H. (2021). Robust multiphase and multilayer starch/polymer (TPS/PBAT) film with simultaneous oxygen/moisture barrier properties. *Journal of Colloid and Interface Science, 593*, 290–303. https://doi.org/10.1016/j.jcis.2021.03.010

Cozzolino, C. A., Cerri, G., Brundu, A., & Farris, S. (2014). Microfibrillated cellulose (MFC): Pullulan bionanocomposite films. *Cellulose, 21*, 4323–4335. https://doi.org/10.1007/s10570-014-0433-x

Constantia Flexibles Group GmbH, 2022. https://consumer.cflex.com/products/ecolam/. (Accessed October 2022).

Cozzolino, C. A., Campanella, G., Ture, H., Olsson, R. T., & Farris, S. (2016a). Microfibrillated cellulose and borax as mechanical, O_2-barrier, and surface-modulating agents of pullulan biocomposite coatings on BOPP. *Carbohydrate Polymers, 143*, 179–187. https://doi.org/10.1016/j.carbpol.2016.01.068

Cozzolino, C. A., Castelli, G., Trabattoni, S., & Farris, S. (2016b). Influence of colloidal silica nanoparticles on pullulan-coated BOPP film. *Food Packaging and Shelf Life, 8*, 50–55. https://doi.org/10.1016/j.fpsl.2016.03.003

Di Bartolo, A., Infurna, G., & Dintcheva, N. T. (2021). A review of bioplastics and their adoption in the circular economy. *Polymers, 13*, 1229. https://doi.org/10.3390/polym13081229

Dilkes-Hoffman, L., Lane, J. L., Grant, T., Pratt, S., Lant, P. A., & Laycock, B. (2018). Environmental impact of biodegradable food packaging when considering food waste. *Journal of Cleaner Production, 180*, 325–334. https://doi.org/10.1016/j.jclepro.2018.01.169

European Commission, 2018. A European Strategy for Plastics in a Circular Economy. Communication from the Commission to the European Parliament, the Council, the European Economic and Social Committee and the Committee of the Regions. Brussels, January 16th 2018 COM (2018). Available online: https://environment.ec.europa.eu/strategy/plastics-strategy_en. (Accessed October 2022).

Faraca, G., & Astrup, T. F. (2019). Plastic waste from recycling centres: Characterisation and evaluation of plastic recyclability. *Waste Management, 95*, 388–398. https://doi.org/10.1016/j.wasman.2019.06.038

Farris, S., Introzzi, L., & Piergiovanni, L. (2009a). Evaluation of a bio-coating as a solution to improve barrier, friction and optical properties of plastic films. *Packaging Technology and Science, 22*, 69–83. https://doi.org/10.1002/pts.826

Farris, S., Cozzolino, C. A., Introzzi, L., & Piergiovanni, L. (2009b). Effects of different sealing conditions on the seal strength of polypropylene films coated with a bio-based thin layer. *Packaging Technology and Science, 22*, 359–369. https://doi.org/10.1002/pts.861

Farris, S., Unalan, I. U., Introzzi, L., Fuentes-Alventosa, J. M., & Cozzolino, C. A. (2014). Pullulan-based films and coatings for food packaging: Present applications, emerging opportunities, and future challenges. *Journal of Applied Polymer Science, 131*, 40539. https://doi.org/10.1002/app.40539

Farris, S. (2018). Engineering properties of packaging films. In M. W. Siddiqui, M. S. Rahman, & A. A. Wani (Eds.), *Innovative Packaging of Fruits and Vegetables: Strategies for Safety and Quality Maintenance* (pp. 211–226). Apple Academic Press Inc.

Farris, S., Buratti, S., Benedetti, S., Rovera, C., Casiraghi, E., & Alamprese, C. (2021). Influence of two innovative packaging materials on quality parameters and aromatic fingerprint of extra-virgin olive oils. *Foods, 10*, 929. https://doi.org/10.3390/foods10050929

Finnigan, B. (2009). Barrier polymers. In K. L. Yam (Ed.), *The Wiley Encyclopedia of Packaging Technology* (pp. 103–109). John Wiley & Sons, Inc.

Firouzi, D., Foucher, D. A., & Bougherara, H. (2014). Nylon-coated ultra high molecular weight polyethylene fabric for enhanced penetration resistance. *Journal of Applied Polymer Science*, 40350. https://doi.org/10.1002/APP.40350

Fuentes-Alventosa, J. M., Introzzi, L., Santo, N., Cerri, G., Brundu, A., & Farris, S. (2013). Self-assembled nanostructured biohybrid coatings by an integrated 'sol–gel/intercalation' approach. *RSC Advances, 3*, 25086. https://doi.org/10.1039/c3ra45640d

Gore, A. H., & Prajapat, A. L. (2022). Biopolymer nanocomposites for sustainable UV protective packaging. *Frontiers in Materials, 9*, Article 855727. https://doi.org/10.3389/fmats.2022.855727

Green, D. W., & Perry, R. H. (2008). *Perry's Chemical Engineers' Handbook* (8th ed.). New York: Mc- Graw-Hill.

Guerritore, M., Olivieri, F., Castaldo, R., Avolio, R., Cocca, M., Errico, M. E., et al. (2022). Recyclable-by-design mono-material flexible packaging with high barrier properties realized through graphene hybrid coatings. *Resources, Conservation & Recycling, 179*, Article 106126. https://doi.org/10.1016/j.resconrec.2021.106126

Haghighi, H., Licciardello, F., Fava, P., Siesler, H. W., & Pulvirenti, A. (2020). Recent advances on chitosan-based films for sustainable food packaging applications. *Food Packaging and Shelf Life, 26*, Article 100551. https://doi.org/10.1016/j.fpsl.2020.100551

Huang, Z., Guo, Y.-h, Zhang, T.-m, Zhang, X.-h, & Guo, L.-y (2013). Fabrication and characterizations of zeolite b–filled polyethylene composite films. *Packaging Technology and Science, 26*, 1–10. https://doi.org/10.1002/pts.1986

Introzzi, L., Blomfeldt, T. O. J., Trabattoni, S., Tavazzi, S., Santo, N., Schiraldi, A., et al. (2012a). Ultrasound-assisted pullulan/montmorillonite bionanocomposite coating with high oxygen barrier properties. *Langmuir, 28*, 11206–11214. https://doi.org/10.1021/la301781n

Introzzi, L., Fuentes-Alventosa, J. M., Cozzolino, C. A., Trabattoni, S., Tavazzi, S., Bianchi, C. L., et al. (2012b). "Wetting enhancer" pullulan coating for antifog packaging applications. *ACS Applied Materials & Interfaces, 4*, 3692–3700. https://doi.org/10.1021/am300784n

Kim, J.-K., Choi, B., & Jin, J. (2020). Transparent, water-stable, cellulose nanofiber-based packaging film with a low oxygen permeability. *Carbohydrate Polymers, 249*, Article 116823. https://doi.org/10.1016/j.carbpol.2020.116823

Kumar, S., Shukla, A., Baul, P. P., Mitra, A., & Halder, D. (2018). Biodegradable hybrid nanocomposites of chitosan/gelatin and silver nanoparticles for active food packaging applications. *Food Packaging and Shelf Life, 16*, 178–184. https://doi.org/10.1016/j.fpsl.2018.03.008

Lavrykov, S. A., & Ramarao, B. (2012). Thermal properties of copy paper sheets. *Drying Technology, 30*, 297–311. https://doi.org/10.1080/07373937.2011.638148

Luzi, F., Torre, L., Kenny, J. M., & Puglia, D. (2019). Bio- and fossil-based polymeric blends and nanocomposites for packaging: Structure–property relationship. *Materials, 12*, 471. https://doi.org10.3390/ma12030471.

Nuruddin, M., Chowdhury, R. A., Szeto, R., Howarter, J. A., Erk, K. A., Szczepanski, C. R., et al. (2021). Structure−property relationship of cellulose nanocrystal−polyvinyl alcohol thin films for high barrier coating applications. *ACS Applied Materials & Interfaces, 13*, 12472–12482. https://doi.org/10.1021/acsami.0c21525

Pinto, L., Bonifacio, M. A., De Giglio, E., Santovito, E., Cometa, S., Bevilacqua, A., et al. (2021). Biopolymer hybrid materials: Development, characterization, and food packaging applications. *Food Packaging and Shelf Life, 28*, Article 100676. https://doi.org/10.1016/j.fpsl.2021.100676

ProAmpac, 2022. https://www.proampac.com/sustainability/products. (Accessed October 2022).

Risyon, N. P., Othman, S. H., Basha, R. K., & Talib, R. A. (2020). Characterization of polylactic acid/halloysite nanotubes bionanocomposite films for food packaging. *Food Packaging and Shelf Life, 23*, Article 100450. https://doi.org/10.1016/j.fpsl.2019.100450

Rizzo, V., Torri, L., Licciardello, F., Piergiovanni, L., & Muratore, G. (2015). Quality changes of extra virgin olive oil packaged in coloured polyethylene terephthalate bottles stored under different lighting conditions. *Packaging Technology and Science, 27*, 437–448. https://doi.org/10.1002/pts.2044

Rovera, C., Türe, H., Hedenqvist, M. S., & Farris, S. (2020). Water vapor barrier properties of wheat gluten/silica hybrid coatings on paperboard for food packaging applications. *Food Packaging and Shelf Life, 26*, Article 100561. https://doi.org/10.1016/j.fpsl.2020.100561

Santhosh, R., Nath, D., & Sarkar, P. (2021). Novel food packaging materials including plant-based byproducts: A review. *Trends in Food Science & Technology, 118*, 471–489. https://doi.org/10.1016/j.tifs.2021.10.013

Schur Flexibles GmbH, 2022. https://www.schurflexibles.com/our-sustainable-packaging-solutions. (Accessed October 2022).

Shanmugam, R., Mayakrishnan, V., Kesavan, R., Shanmugam, K., Veeramani, S., & Ilangovan, R. (2021). Mechanical, barrier, adhesion and antibacterial properties of pullulan/graphene bio nanocomposite coating on spray coated nanocellulose film for

food packaging applications. *Journal of Polymers and the Environment, 30*, 1749–1757. https://doi.org/10.1007/s10924-021-02311-2

Sharif, U., Sun, B., Islam, M. S., Majeed, K., Ibrahim, D. S., Adewale, O. O., et al. (2021). Fracture toughness analysis of aluminum (Al) foil and its adhesion with low-density polyethylene (LPDE) in the packing industry, 1079. 9 *Coatings, 11*. https://doi.org/10.3390/coatings11091079.

Song, H.-g, Choi, I., Lee, J.-S., Chang, Y., Yoon, C. S., & Han, J. (2022). Whey protein isolate coating material for high oxygen barrier properties: A scale-up study from laboratory to industrial scale and its application to food packaging. *Food Packaging and Shelf Life, 31*, Article 100765. https://doi.org/10.1016/j.fpsl.2021.100765

Trossaert, L., De Vel, M., Cardon, L., & Edeleva, M. (2022). Lifting the sustainability of modified pet-based multilayer packaging material with enhanced mechanical recycling potential and processing. *Polymers, 14*, 196. https://doi.org/10.3390/polym14010196

Tyagi, P., Salem, K. S., Hubbe, M. A., & Pal, L. (2021). Advances in barrier coatings and film technologies for achieving sustainable packaging of food products – A review. *Trends in Food Science & Technology, 115*, 461–485. https://doi.org/10.1016/j.tifs.2021.06.036

Tyun'kin, I. V., Bazhenov, S. L., Efimov, A. V., Kechek'yan, A. S., & Timan, S. A. (2011). The effect of orientation on the mechanism of deformation of polymers. *Polymer Science, Series A, 53*, 715–726. https://doi.org/10.1134/S0965545×11080116

Unalan, I. U., Boyaci, D., Ghaani, M., Trabattoni, S., & Farris, S. (2016). Graphene oxide bionanocomposite coatings with high oxygen barrier properties. *Nanomaterials, 6*, 244–254. https://doi.org/10.3390/nano6120244

Wang, J., Gardner, D. J., Stark, N. M., Bousfield, D. W., Tajvidi, M., & Cai, Z. (2018). Moisture and oxygen barrier properties of cellulose nanomaterialbased films. *ACS Sustainable Chemistry & Engineering, 6*, 49–70. https://doi.org/10.1021/acssuschemeng.7b03523

Wipak Group, 2022. https://www.wipak.com/green-choice/recyclable. (Accessed October 2022).

Wu, C., Zhu, Y., Wu, T., Wang, L., Yuan, Y., Chen, J., et al. (2019). Enhanced functional properties of biopolymer film incorporated with curcumin-loaded mesoporous silica nanoparticles for food packaging. *Food Chemistry, 288*, 139–145. https://doi.org/10.1016/j.foodchem.2019.03.010

Zarandi, M. B., Bioki, H. A., Mirbagheri, Z.-a, Tabbakh, F., & Mirjalili, G. (2012). Effect of crystallinity and irradiation on thermal properties and specific heat capacity of LDPE & LDPE/EVA. *Applied Radiation and Isotopes, 70*, 1–5. https://doi.org/10.1016/j.apradiso.2011.09.001

Zia, J., Paul, U. C., Heredia-Guerrero, J. A., Athanassiou, A., & Fragouli, D. (2019). Low-density polyethylene/curcumin melt extruded composites with enhanced water vapor barrier and antioxidant properties for active food packaging. *Polymer, 175*, 137–145. https://doi.org/10.1016/j.polymer.2019.05.012